

# Modelling magnetism of C at O and B monovacancies in graphene

T. P. Kaloni<sup>1</sup>, M. Upadhyay Kahaly<sup>1</sup>, R. Faccio<sup>2,3</sup>, and U. Schwingenschlög<sup>1,\*</sup>

<sup>1</sup>*PSE Division, KAUST, Thuwal 23955-6900, Kingdom of Saudi Arabia*

<sup>2</sup>*Crystallography, Solid State and Materials Laboratory (Cryssmat-Lab),*

*DETEMA, Facultad de Química, Universidad de la República,*

*Gral. Flores 2124, P.O. Box 1157, Montevideo, Uruguay*

<sup>3</sup>*Centro NanoMat, Polo Tecnológico de Pando,*

*Facultad de Química, Universidad de la República,*

*Cno. Aparicio Saravia s/n, 91000, Pando, Canelones, Uruguay*

## Abstract

The presence of defects can introduce important changes in the electronic structure of graphene, leading to phenomena such as C magnetism. In addition, vacancies are reactive and permit the incorporation of dopants. This paper discusses the electronic properties of defective graphene for O and B decoration. Phonon calculations allow us to address directly the stability of the systems under study. We show that it is possible to obtain magnetic solutions with and without dangling bonds, demonstrating that C magnetism can be achieved in the presence of B and O.

---

\*Electronic address: Corresponding author. Tel.: +966 544700080. E-mail address: udo.schwingenschlogl@kaust.edu.sa (U. . .)

## 1. Introduction

C nanostructures have attracted the attention of the scientific community because of both unique fundamental properties and potential in technological applications. In particular, the high coherence length and large conductivity [1] of C materials are promising in electronics and spintronics. On the other hand, also magnetism has been observed in this class of materials [2], generating huge interest of both experiment and theory [3–9]. The structural, electronic, and magnetic properties of defective graphene have been studied in detail and it has been confirmed that vacancies are the source of magnetism [10–13]. It has been demonstrated that point defects lead to notable paramagnetism but no magnetic ordering is achieved down to liquid helium temperature [14]. In addition, the point defects carry magnetic moments irrespective of the vacancy concentration. In [15] the authors report that the extended  $\pi$ -band magnetism reduces to zero in the limit of monovacancies in graphene. For these reasons, it is important to evaluate the role of saturation and chemical modifications in the neighborhood of mono and multivacancies in order to understand how a persistent magnetic ordering can be achieved.

Graphene samples in general are characterized by the presence of  $sp^2$  hybridized C atoms, extended pores, and various attached functional groups, as revealed by scanning electron microscopy, atomic force microscopy, and Raman spectroscopy. It has been concluded that the appearance of magnetism requires the presence of defects, adatoms, or topological defects [16]. Zagaynova and coworkers have prepared magnetic C by chemical oxidation [17]. B doping in general leads to different magnetic responses depending on the amount of doping. This behavior has been partially addressed by Faccio and coworkers [18], who have demonstrated that magnetism requires the proximity of B and a monovacancy. However, when the B atom is too close to the vacancy all the dangling bonds are reconstructed and magnetism is suppressed. The authors of [19] have addressed the situation of multiple O atoms attached to a monovacancy in graphene, demonstrating that vacancies are magnetic if and only if they are metallic and non-magnetic if and only if they are semiconducting. Metallicity and magnetism thus are simultaneously determined by the presence or absence of dangling C bonds after the oxidation. In our present work, we give a theoretical study of the effects of vacancies interacting with different amounts of B and O atoms, focusing on the structural, electronic, and magnetic properties. An experimental realization of the proposed structures is possible along the lines of Ref. [20].

## 2. Methods

We employ density functional theory in the generalized gradient approximation (Perdew-Burke-Ernzerhof scheme) as implemented in the Quantum-ESPRESSO code [21]. All calculations are performed with a plane wave cutoff energy of 544 eV. A Monkhorst-Pack  $8 \times 8 \times 1$  k-mesh is used to relax the structures and a  $16 \times 16 \times 1$  k-mesh to calculate the density of states (DOS) with a high accuracy. We use a  $5 \times 5$  supercell of pristine graphene in our calculations [22]. This supercell size has shown in various studies to be sufficient for functionalization of graphene by atoms, small molecules, amine and nitrobenzene groups, and others [23–28]. Our supercell contains 50 C atoms and has a lattice constant of  $a = 12.2$  Å with a 20 Å thick vacuum layer on top. The atomic positions are relaxed upto an energy convergence of  $10^{-7}$  eV and a force convergence of  $0.005$  eV/Å. For our vibrational study, the phonon frequencies and eigenvectors at the  $\Gamma$ -point are calculated with an energy error of less than  $10^{-14}$  eV. Phonon frequencies at the  $\Gamma$ -point are determined by density functional perturbation theory for evaluating the structural stability [29]. We note that the numerics break the symmetry of the dynamical matrix and introduce slight errors in the phonon frequencies of maximal  $15$   $\text{cm}^{-1}$ , which, however, are not critical.

In a first step, we create a monovacancy in our  $5 \times 5$  supercell and relax the system. Afterwards, we add O and B atoms in the vicinity of the monovacancy for different starting geometries and relax the system again. Several prototypical monovacancies are prepared in order to consider various possibilities with different O and B concentrations. We name these configurations giving first the number of O atoms and second the number of B atoms. For example, configuration 1/2 has 1 O and 2 B atoms in the vicinity of the monovacancy. All the configurations under study are shown in Figs. 1 and 2. Note that we have tested the required supercell size by addressing for the most stable configurations  $10 \times 10$  supercells and find no significant modification in the induced buckling of the graphene sheet after O and B adsorption.

## 3. Results and discussion

At a clean monovacancy the under-coordinated C atom is subject to Jahn-Teller distortion [30] and therefore moves out of the graphene plane by  $0.13$  Å. We find a total magnetic moment of  $1.35 \mu_B$ , where  $1 \mu_B$  is due to the localized dangling bond of one C atom and the remaining moment is carried by extended  $\pi$  states [19]. The vacancy formation energy,

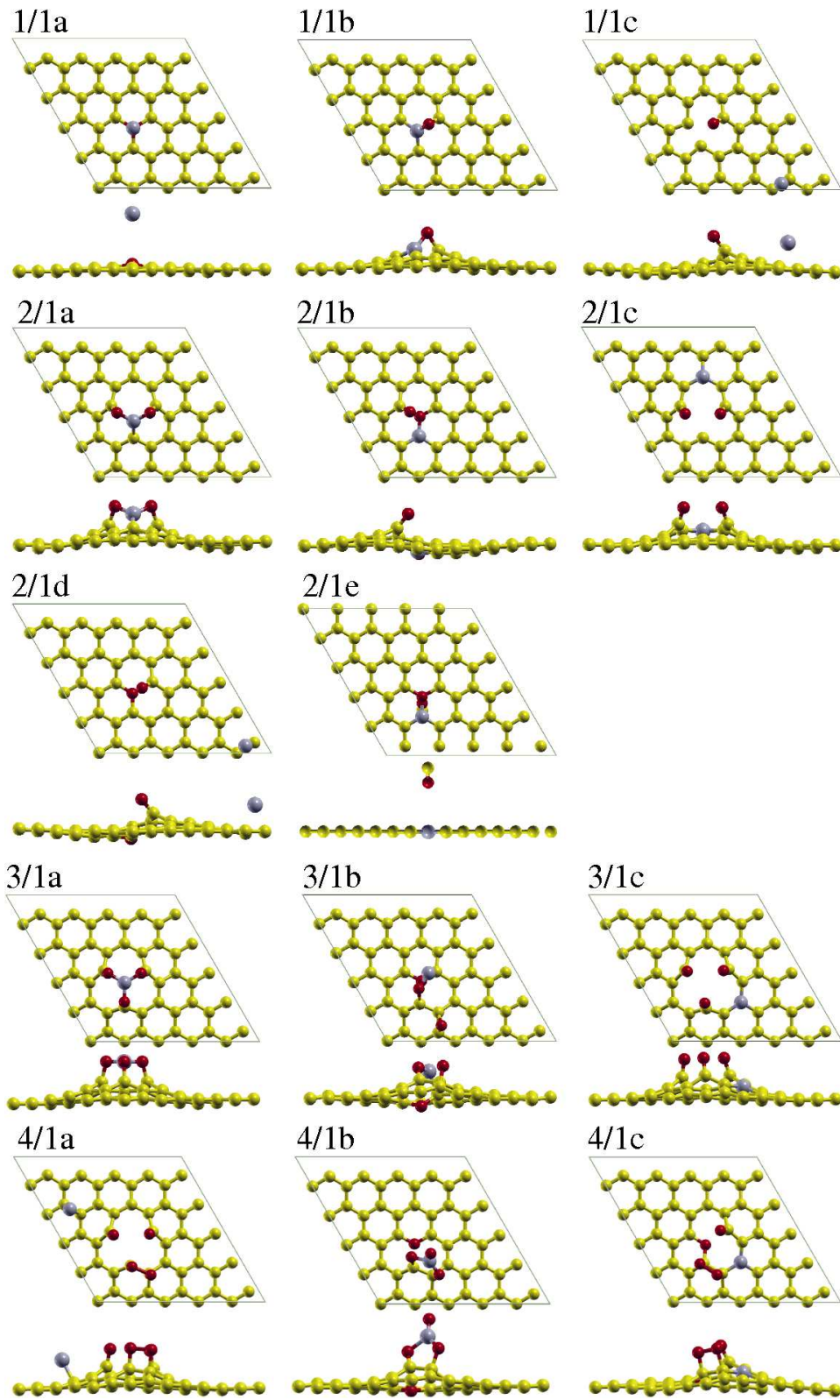


FIG. 1: Crystal structures for 1 B and 2, 3, or 4 O atoms adsorbed at a monovacancy in graphene. The yellow, red, and gray spheres represent C, O, and B, respectively.

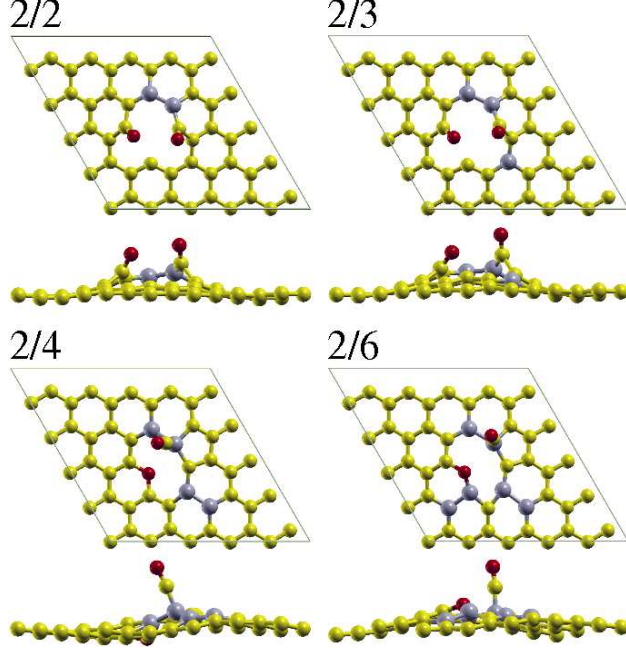


FIG. 2: Crystal structures for 2 O and 2, 3, 4, or 6 B atoms adsorbed at a monovacancy in graphene. The yellow, red, and gray spheres represent C, O, and B, respectively.

$E_{form}$ , is determined by the expression

$$E_{form} = E_{vacancy} - \frac{N-1}{N} E_{graphene}, \quad (1)$$

where  $E_{vacancy}$  and  $E_{graphene}$  are the total energies of defective and pristine graphene, respectively. Moreover,  $N$  is the number of atoms in the pristine graphene. The obtained value of  $E_{form}$  is 7.4 eV, which agrees well with previous reports [31, 32].

We first study a monovacancy decorated by 1 O atom to which 1 B atom is added. When forcing the O atom to occupy a position within the graphene plane connected to 3 C atoms the B atom is released and repelled, leading to configuration 1/1a. In configuration 1/1b the B atom connects to 1 O atom and 2 C atoms, saturating all dangling bonds. Moreover, configuration 1/1c deals with B adsorption far from the vacancy, for which we obtain a bridge position over a C–C bond with  $d_{B-C} = 1.87 \text{ \AA}$ . The energetics of the doping process indicate that the chemical reaction between graphene-oxide and B can be evaluated as

$$E_{form} = E_{vacancy+B+O} - \frac{N-N_C}{N} E_{graphene} - \frac{N_O}{2} E_{O_2} - N_B E_{B,bulk}, \quad (2)$$

where  $E_{vacancy+B+O}$  is the total energy after B adsorption on graphene-oxide. In addition,  $N_C$ ,  $N_O$ , and  $N_B$  are the numbers of missing C atoms and additional O and B atoms in

System	$E_{form}$ (eV)	Magnetic moment ( $\mu_B$ )
1/1a	-1.7	1.0
1/1b	-6.9	0.2
1/1c	-1.7	0.0
2/1a	-7.0	0.0
2/1b	-7.4	0.1
2/1c	-5.3	1.0
2/1d	-4.8	0.0
2/1e	-6.9	0.5*
3/1a	-4.4	0.2
3/1b	-3.4	1.0
3/1c	-3.5	1.0
4/1a	1.1	0.0
4/1b	-11.3	0.0
4/1c	1.6	0.0
2/2	-8.4	1.0
2/3	-12.8	1.0
2/4	-22.9	0.0
2/6	-34.4	0.0

TABLE I: Formation energy and magnetic moment. \*The magnetic moment is located on the released CO molecule.

the decorated system. It turns out that configuration 1/1b is energetically favorable with  $E_{form} = -6.9$  eV, see Table I, while for configurations 1/1a and 1/1c we obtain in each case a value of  $-1.7$  eV. By the huge energy difference it is clear that only configuration 1/1b will be realized. Due to the B adsorption and the induced C and O reconstructions, this configuration becomes a metal, see Fig. 3(a). The Dirac cone, which is still due to the C  $p_z$  orbitals with no contribution of O or B, splits and shifts above  $E_F$  by about 0.6 eV. Interestingly, a magnetic moment of  $0.2 \mu_B$  is observed although no dangling bonds are present.

Turning to an oxidized monovacancy decorated by 2 O atoms, in configuration 2/1a the B

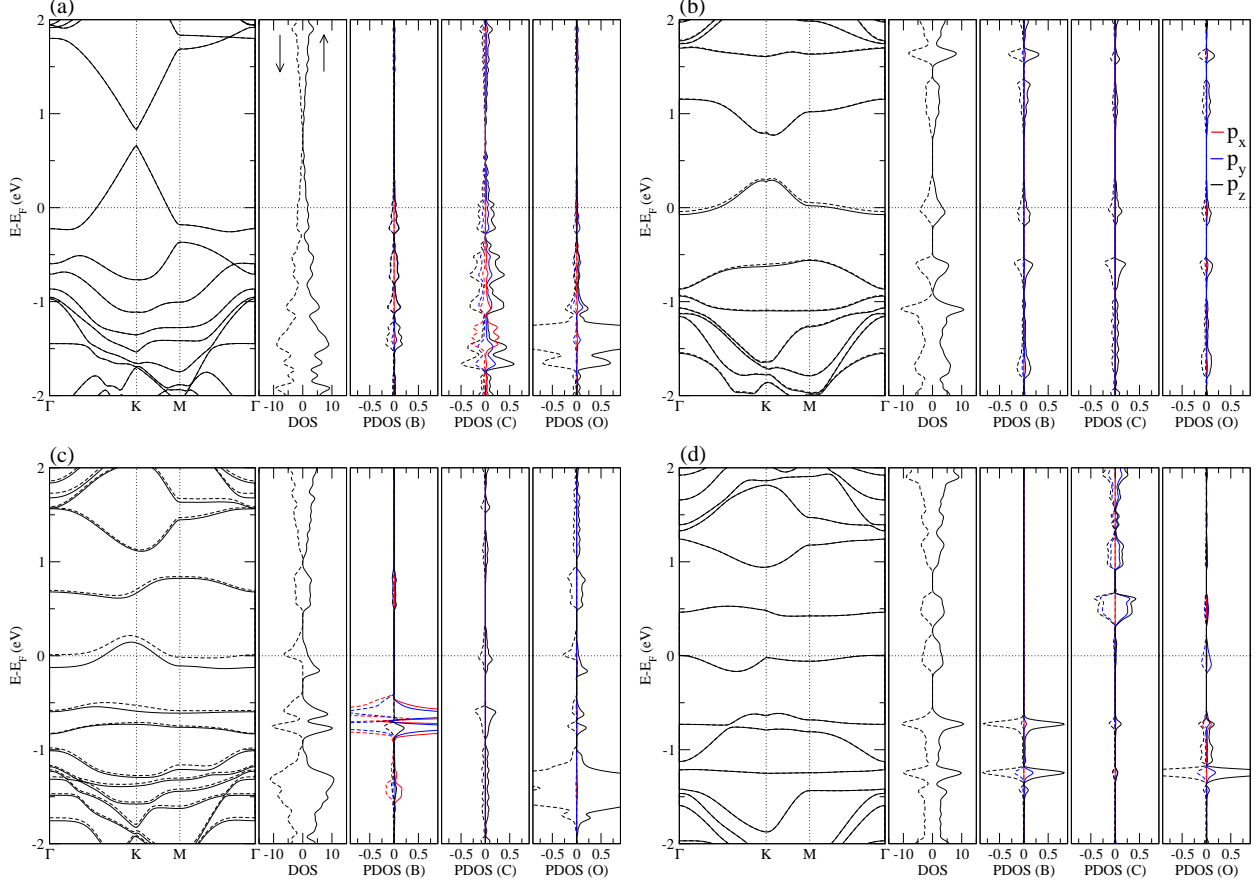


FIG. 3: Electronic band structure and DOS for the structures (a) 1/1b, (b) 2/1b, (c) 3/1a, and (d) 4/1b.

atom establishes strong interaction with O and C, which originally was under-coordinated. We obtain  $E_{form} = -7.0$  eV and no spin polarization due to saturation of all dangling C bonds. In configurations 2/1b and 2/1c the B atom is adsorbed at the boundary of the vacancy, leading to reconstructions with one and two C=O bonds, respectively. We obtain for  $E_{form}$  values of  $-7.4$  eV and  $-5.3$  eV, where configuration 2/1c is less favorable due to the presence of a dangling C bond which induces a magnetic moment of  $1 \mu_B$ . In configuration 2/1d the B atom is adsorbed far away from the monovacancy, which yields a surprising geometrical reconstruction: the two C=O bonds change into one ketone (C=O) and one ether group. However, with  $E_{form} = -4.8$  eV this configuration is not favorable. Finally, in configuration 2/1e the B atom is located in the graphene plane and a CO molecule is released. We obtain  $E_{form} = -6.9$  eV. In Fig. 3(b) we address the electronic band structure of the energetically favorable configuration 2/1b. We find that one spin majority band and

one spin minority band cross  $E_F$ , both contributed by the C  $p_z$  orbitals. The semiconducting state of a monovacancy decorated by 2 O atoms is transferred into a metallic state by B adsorption.

For B adsorption at a monovacancy decorated by 3 O atoms, configuration 3/1a is characterized by three ketone groups, establishing a  $\text{BO}_3$  unit with an interatomic distance of  $d_{B-O} = 1.38 \text{ \AA}$ . In configuration 3/1b the B atom is attached to one ketone group and one C terminated ether group, which changes the original  $sp^2$  hybridization into a  $sp^3$  hybridization, with interatomic distances of  $d_{B-O} = 1.35 \text{ \AA}$  and  $d_{B-C} = 1.62 \text{ \AA}$ . Since in configuration 3/1c the B atom substitutes a C atom near the vacancy, the structure does not change significantly. Configuration 3/1a is clearly favorable with  $E_{form} = -4.4 \text{ eV}$ , as compared to values of  $-3.4 \text{ eV}$  and  $-3.5 \text{ eV}$  for configurations 3/1b and 3/1c. For configuration 3/1a we find a magnetic moment of  $0.6 \mu_B$ . In addition, Fig. 3(c) shows that this configuration 3/1a is metallic with two distinct C  $p_z$  derived bands crossing  $E_F$ . The observed localized states can be attributed to the under-coordination of the B atom, which clearly distinguishes this case from configurations 3/1b and 3/1c.

In the case of 4 adsorbed O atoms, three configurations are found to be stable. Configuration 4/1a has two ketone groups and one peroxide ( $-\text{O}-\text{O}-$ ) group and configuration 4/1b one ketone, one peroxide, and one ether group. The origin of the stability is the fact that the  $\text{BO}_3$  group itself is very stable [33]. In the former case the B atom is adsorbed far away from to the monovacancy, while in the latter it bonds with the 2 O atoms to form a  $\text{BO}_3$  group. Configuration 4/1c is similar to configuration 4/1a but with B substituting C at the boundary of the vacancy. Regarding the energetics, configuration 4/1b is strongly favorable with  $E_{form} = -11.3 \text{ eV}$ , as compared to values of  $1.1 \text{ eV}$  and  $1.6 \text{ eV}$ , since a peroxide group is present. The electronic structure shown in Fig. 3(d) indicates that this configuration is semiconducting with a band gap of  $0.5 \text{ eV}$  at the K point, and not magnetic.

We next evaluate the effect of the B concentration on the electronic structure of oxidized graphene by substituting 2 to 6 B atoms on C sites for a fixed O concentration (two adsorbed O atoms), see Fig. 2. In configuration 2/2 two B atoms replace two C atoms at the boundary of the vacancy. The system develops a magnetic moment of  $1 \mu_B$  due to the presence of a dangling C bond. In configuration 2/3 the substitution of an additional B atom does not change this situation. The fourth B atom in configuration 2/4 establishes a linear  $\text{B}-\text{C}=\text{O}$  bond, which is similar to the bond evolving in configuration 2/6.  $E_{form}$  varies strongly

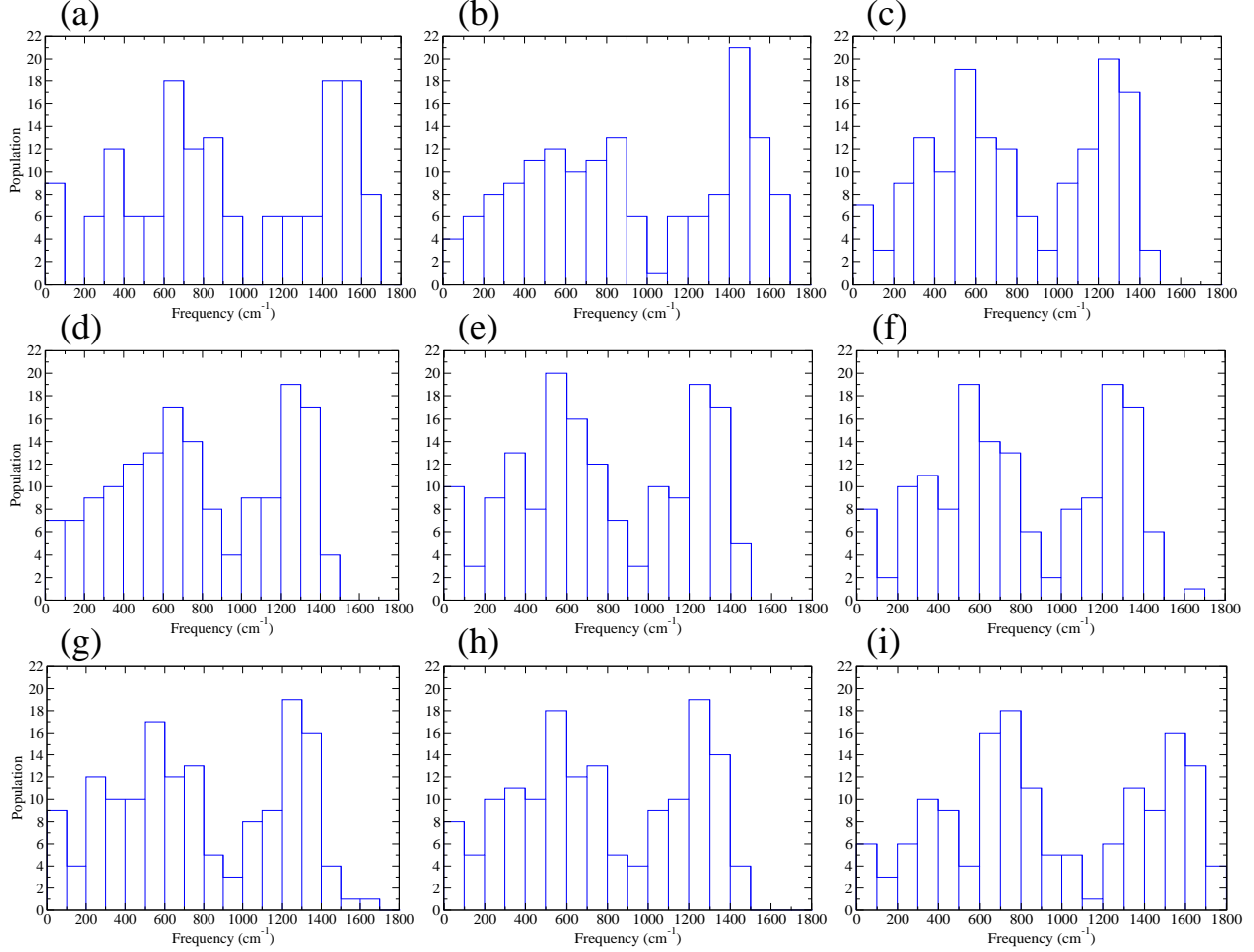


FIG. 4: Phonon frequency at the  $\Gamma$ -point for (a) pristine graphene, the structures (b) 1/1b, (c) 2/1b, (d) 3/1a, (e) 4/1b, (f) 2/2, (g) 2/4, (h) 2/6, and (i) 2 O atoms adsorbed at a monovacancy.

between  $-8.4$  eV and  $-34.4$  eV due to the formation of B–B dimers. Our results show that there is a strong tendency to B adsorption at oxidized monovacancies.

We note the appearance of fractional magnetic moments in several cases:  $0.1 \mu_B$  in configuration 2/1b and  $0.2 \mu_B$  in configurations 1/1b and 3/1a. For the remaining systems the moment is either 0 or  $1 \mu_B$ , see Table I, and therefore results from localized dangling bonds. In all systems with fractional moments there are no contributions of the adsorbed O and/or B atoms to the magnetization. Spin polarization is carried only by C atoms, where the atoms forming the boundary of the defect contribute less than those further away. While clean monovacancies in graphene do not give rise to extended  $\pi$ -band magnetism, the situation changes under O and B decoration.

The calculation of  $\Gamma$ -point phonons allows us to address the structural stability after

O and B doping. Phonon densities of states are shown as histograms for the most stable structures (1/1b, 2/1b, 3/1a, 4/1b, 2/2, 2/4, 2/6) in Fig. 4 together with results for pristine graphene and for 2 O atoms adsorbed at a monovacancy. Note that the reported frequencies refers to the  $\Gamma$ -point of the Brillouine zone of our  $5 \times 5$  supercell and due to backfolding therefore also include frequencies of other points of the standard graphene Brillouin zone. This phenomenon is well-known from carbon nanotubes [34–38]. We find all phonon frequencies to be positive and therefore conclude that all configurations addressed in Fig. 4 are stable. Pristine graphene shows a two peak phonon spectrum, where the gross shape is largely maintained under O and B adsorption. This finding is consistent with recent experimental results of Raman spectroscopy of B doped graphene [39]. However, there are characteristic differences evident in the high frequency range beyond  $1500 \text{ cm}^{-1}$ . Except for configuration 1/1b, the modes in this energy range are suppressed and the high frequency peak shifts to the left. This fact cannot be a consequence of O adsorption, since an oxidized monovacancy without adsorbed B atoms rather comes along with an enhancement of the high energy modes, see Fig. 4(i). The softening of the G modes appears to be related to out-of-plane shifts of O atoms and substantial local distortions in the graphene plane induced by B adsorption.

#### 4. Conclusion

We have performed first principles calculations to study the structural, electronic, and magnetic properties of O and B decorated graphene. We have identified the energetically favorable configurations for a variety of O and B concentrations and have demonstrated that there exist magnetic solutions with and without dangling bonds. Since vacancies in graphene are reactive and permit the incorporation of dopants, our calculations demonstrate that B doping of oxidized vacancies is a successful approach to induce extended  $\pi$ -band magnetism. By controlling the O and B concentrations, it is even possible to tune the magnetic state. A study of the  $\Gamma$ -point phonons has been performed to understand the structural stability of the decorated monovacancies.

#### Acknowledgments

We thank KAUST research computing for providing the computational resources used for this investigation. M. Upadhyay Kahaly thanks SABIC for financial support. R. Faccio thanks the PEDECIBA, CSIC, and Agencia Nacional de Investigación e Innovación (ANII) Uruguayan organizations for financial support.

## References

---

- [1] Castro Neto AH, Guinea F, Peres NMR, Novoselov KS, Geim AK. The electronic properties of graphene. *Rev. Mod. Phys.* 2009; 81: 109-162.
- [2] Makarova T, Palacio F. C-based magnetism: An overview of metal free C-based compounds and materials. Amsterdam: Elsevier. 2005.
- [3] Esquinazi P, Setzer A, Höhne R, Semmelhack C, Kopelevich Y, Spemann D, et al. Ferromagnetism in oriented graphite samples. *Phys. Rev. B* 2002; 66: 024429.
- [4] Esquinazi P, Spemann D, Höhne R, Setzer A, Han KH, T. Butz. Induced magnetic ordering by proton irradiation in graphite. *Phys. Rev. Lett.* 2003; 91: 227201.
- [5] Rode AV, Gamaly EG, Christy AG, Gerald JGF, Hyde ST, Elliman RG, et al. Unconventional magnetism in all-carbon nanofoam. *Phys. Rev. B* 2004; 70: 054407.
- [6] Lehtinen PO, Foster AS, Ma Y, Krasheninnikov AV, Nieminen RM. Irradiation-induced magnetism in graphite: A density functional study. *Phys. Rev. Lett.* 2004; 93: 187202.
- [7] Črvenka JS, Katsnelson MI, Flipse CFJ. Room-temperature ferromagnetism in graphite driven by two-dimensional networks of point defects. *Nat. Phys.* 2009; 5: 840-844.
- [8] Ugeda MM, Brihuega I, Guinea F, Gómez-Rodríguez JM. Missing atom as a source of carbon magnetism. *Phys. Rev. Lett.* 2010; 104: 096804.
- [9] Kaloni TP, Upadhyay Kahaly M, Schwingenschlögl U. Induced magnetism in transition metal intercalated graphitic systems. *J. Mater. Chem.* 2011; 21: 18681-18685.
- [10] Singh R, Kroll P. Magnetism in graphene due to single-atom defects: Dependence on the concentration and packing geometry of defects. *J. Phys.: Condens. Matter* 2009; 21: 196002.
- [11] Nanda BKR, Sherafati M, Popovic Z, Satpathy S. Electronic structure of the substitutional vacancy in graphene: Density-functional and Green's function studies. *New J. Phys.* 2012; 14: 083004.
- [12] Yang X, Xia H, Qin X, Li W, Dai Y, Liu X et al. Correlation between the vacancy defects and ferromagnetism in graphite. *Carbon* 2009; 47: 1399.
- [13] Lim DH, Negreira AS, Wilcox J. DFT Studies on the interaction of defective graphene-supported Fe and Al nanoparticles. *J. Phys. Chem. C* 2011; 115: 8961.
- [14] Nair RR, Sepioni M, Tsai IL, Lehtinen O, Keinonen J, Krasheninnikov AV, et al. Spin-half

- paramagnetism in graphene induced by point defects. *Nat. Phys.* 2012; 8: 199-202.
- [15] Palacios JJ, Ynduráin F. Critical analysis of vacancy-induced magnetism in monolayer and bilayer graphene. *Phys. Rev. B* 2012; 85: 245443.
- [16] Pardo H, Khane ND, Faccio R, Araújo-Moreira FM, Fernández-Werner L, Makarova T, et al. Raman characterization of bulk ferromagnetic nanostructured graphite. *Physica B: Cond. Matt.* 2012; 407; 3206-3209.
- [17] Zagaynova VS, Makarova TL, Bergstrom L, Vasiliev P, Araújo-Moreira FM, Pardo H, et al. Boron doped graphene oxide. Submitted (2012).
- [18] Faccio R, Fernández-Werner L, Pardo H, Goyenola C, Ventura ON, Mombrú AW. Electronic and structural distortions in graphene induced by carbon vacancies and boron doping. *J. Phys. Chem. C* 2010; 114: 18961-18971.
- [19] Kaloni TP, Cheng YC, Faccio R, Schwingenschlögl U. Oxidation of monovacancies in graphene by oxygen molecules. *J. Mater. Chem.* 2011; 21: 18284-18288.
- [20] Pardo H, Faccio R, Araujo-Moreira FM, Lima de OF, Mombru WA. Synthesis and characterization of stable room temperature bulk ferromagnetic graphite. *Carbon* 2006; 44: 565.
- [21] Giannozzi P, Baroni S, Bonini N, Calandra M, Car R, Cavazzoni C, et al. Quantum ESPRESSO: a modular and open-source software project for quantum simulations of materials. *J. Phys.: Condens. Matter* 2009; 21: 395502.
- [22] Cheng YC, Kaloni TP, Zhu ZY, Schwingenschlögl U. Oxidation of graphene in ozone under ultraviolet light. *Appl. Phys. Lett.* 2012; 101: 073110.
- [23] Saha KS, Chandrakanth RC, Krishnamurthy HR, Waghmare UV. Mechanisms of molecular doping of graphene: A first-principles study. *Phys. Rev. B* 2009; 80: 155414.
- [24] Johari P, Shenoy VB. Modulating optical properties of graphene oxide: Role of prominent functional groups. *ACS Nano* 2011; 5: 7640.
- [25] Dai J, Yuan J, Giannozzi P. Gas adsorption on graphene doped with B, N, Al, and S: A theoretical study. *Appl. Phys. Lett.* 2009; 95: 232105.
- [26] Yan J-A, XianL, Chou MY. Structural and electronic properties of oxidized graphene. *Phys. Rev. Lett.* 2009; 103: 086802.
- [27] Wu M, Cao C, Jiang JZ. Electronic structure of substitutionally Mn-doped graphene. *New J. Phys.* 2010; 12: 063020.
- [28] Wu B-R, Yang C-K. Electronic structures of graphane with vacancies and graphene adsorbed

- with fluorine atoms. *AIP Advances* 2012; 2: 012173.
- [29] Baroni S, de Gironcoli S, Dal Corso A. Phonons and related crystal properties from density-functional perturbation theory. *Rev. Mod. Phys.* 2001; 73: 515-562.
- [30] Jahn A, Teller E. Stability of polyatomic molecules in degenerate electronic states. I. Orbital degeneracy. *Proc. R. Soc. Lond. A* 1937; 61: 220-235.
- [31] Banhart F, Kotakoski J, Krasheninnikov AV. Structural defects in graphene. *ACS Nano* 2011; 5: 26-41.
- [32] El-Barbary AA, Telling RH, Ewels CP, Heggie MI, Briddon PR. Structure and energetics of the vacancy in graphite. *Phys. Rev. B* 2003; 68: 144107.
- [33] Sheng ZH, Gao HJ, Bao WJ, Wang FB, Xia XH. Synthesis of boron doped graphene for reduction reaction in fuel cells. *J. Mater. Chem.* 2012; 22: 390.
- [34] Marconcini P and Macucci M. A novel choice of the graphene unit vectors, useful in zone-folding computations. *Carbon* 2007; 45: 1018.
- [35] Kahaly MU, Waghmare UV. Vibrational properties of single-wall carbon nanotubes: A first-principles study. *J. Nanosci. Nanotechnol.* 2007; 7: 1787.
- [36] Maultzsch J, Reich S, Thomsen C, Dobardzic E, Milosevic I, Damnjanovic M. Phonon dispersion of carbon nanotubes. *Solid State Commun.* 2002; 121: 471.
- [37] Saito R, Takeya T, Kimura T, Dresselhaus G, Dresselhaus MS. Raman intensity of single-wall carbon nanotubes. *Phys. Rev. B* 1998; 57: 4145.
- [38] Doorn SK, Zheng L, O'Connell MJ, Zhu Y, Huang S, Liu J. Raman spectroscopy and imaging of ultralong carbon nanotubes. *Phys. Chem.* 2005; 109: 3751.
- [39] Kim YA, Fujisawa K, Muramatsu H, Hayashi T, Endo M, Fujimori T et al. Raman spectroscopy of boron-doped single-layer graphene. *ACS Nano* 2012; 6: 6293.